Reprinted from Preprint Volume: Conference on Cloud Physics and Atmospheric Electricity, July 31-August 4, 1978, Issaquah, Wash. Published by The American Meteorological Society, Boston, Mass.

13.2

MESOSCALE VERTICAL AIR MOTIONS IN INTENSE TROPICAL CONVECTION

Colleen A. Leary and Robert A. Houze, Jr.

Department of Atmospheric Sciences
University of Washington
Seattle, Washington 98195

1. INTRODUCTION

Abercromby (1887) was perhaps the first to document the anomalously low surface temperatures observed to the rear of an intense squall line and suggest that they were due to the transport downward of cold air with heavy rain. Humphreys (1914) identified the evaporation of falling rain as the dominant mechanism for the cooling as well as the source of the downdrafts in a thunderstorm. He also noted two distinct rain areas in the thunderstorm: a primary rain area located close to the ascending air, and a less intense secondary rain area well to the rear of the ascending air and the primary rain area. In the tropics, Hamilton and Archbold (1945) described similar phenomena in squall lines, which they called disturbance lines, and associated the light rain area to the rear of the most intense showers with a deep anvil of altostratus cloud.

Zipser (1969, 1977) deduced the presence of an organized mesoscale downdraft driven by the evaporation of falling precipitation beneath the deep altostratus layer in the rear portion of tropical squall-line systems. He distinguished this mesoscale downdraft from the convective-scale downdrafts at the leading edge of the system. Motivated by Zipser's (1969) study, Brown (1974) constructed a two-dimensional, time-dependent numerical model of a precipitating tropical disturbance, using the unfiltered hydrostatic equations, together with parameterizations of cloud microphysics and convective-scale motions. His experiments showed that a mesoscale downdraft developed only when evaporation due to falling rain was included in the calculations, and when the wind shear was sufficiently great to displace the falling rain from the zone of uplift due to cumulus-scale updrafts. Above the mesoscale downdraft, his model produced a region of mesoscale uplift in a deep cloud layer similar to the anvil cloud observed in squall-line systems.

The importance of the precipitation falling in the anvil region of observed tropical squall-line systems has been documented by Houze (1977), who found that 40% of the total precipitation in a squall-line system fell in the anvil region. He also deduced the presence of a mesoscale downdraft beneath the anvil cloud. Leary and Houze (1978a) inferred the presence of mesoscale downdrafts not only in squall-line systems, but also in two cases of intense non-squall mesoscale precipitation features in the tropics. In addition, they calculated cooling rates of 1-5°C h^{-1} at the melting level in the region of horizontally uniform precipitation beneath the anvil cloud. Their calculations suggest that cooling due to the melting of hydrometeors, in addition to evaporative cooling, plays an important role in the initiation and maintenance of mesoscale downdrafts in intense convective systems.

Diagnostic studies of the mass and heat budgets in intense tropical convective systems have so far assumed that all the precipitation in such systems is associated with convective-scale updrafts and downdrafts (Yanai *et al.*, 1973; Houze and Leary, 1976; Johnson, 1976). Since a large quantity of precipitation associated with mesoscale vertical air motions appears to be a characteristic feature of intense tropical convection, the effects of these mesoscale motions on the mass and heat budgets of intense convective systems should no longer be ignored.

2. A HYPOTHETICAL MESOSCALE SYSTEM AND FOUR DIFFERENT SETS OF ASSUMPTIONS REGARDING ITS WATER BUDGET

In order to determine how mesoscale vertical air motions affect the vertical transports of mass and heat in intense convective systems, we formulated a hypothetical mesoscale precipitation system and calculated the vertical transports of mass and heat accomplished by the system under four different sets of assumptions. The mesoscale precipitation system, shown schematically in Fig. 1, closely resembles those described by Houze (1977) and Leary and Houze (1978b,c). It consists of a convective region of intense, cellular precipitation (region C) and a mesoscale region of lighter, horizontally uniform rain (region M). We specify a lifetime of 24 hours for this system and assume that for the first six hours only the convective region is present while for the last six hours only the mesoscale region is present.

We chose four different water budgets for the mesoscale system (Figs. 2-5). In each case, we assume that the same total amount of rain, $R = 4.5 \times 10^{12}$ kg, falls from the system, with 60% falling in region C and 40% in region M. The four budgets differ in the way they explain the mesoscale conponent of the total precipitation, that is, the 0.4R which falls in region M. This mesoscale rain can be generated in only two possible ways. Either water is first condensed in region C and is subsequently transported horizontally to region M where it eventually falls as mesoscale horizontally uniform rain, or the

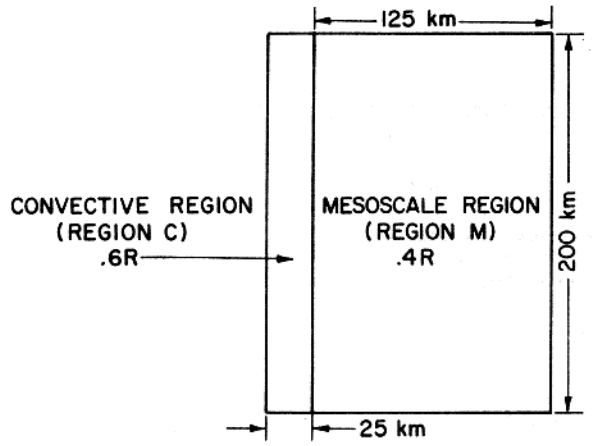

Figure 1. Horizontal dimensions of the hypothetical mesoscale system. R represents 4.5 x 10^{12} kg, the total of precipitation at the surface.

mesoscale rain in region M is generated by mesoscale lifting in the upper troposphere of region M, as predicted in Brown's (1974) model. In the four cases examined here, the mesoscale rain in region M is produced through different combinations of transport from region C to M and mesoscale lifting within region M itself.

a. Case I

Case I (Fig. 2) assumes that all of the precipitation which falls in region M was first condensed in convective-scale updrafts located in region C. For this case to occur, hydrometeors accounting for all 40% of R would have to be transported out of the convective region C and over into the horizontally uniform mesoscale region M. This situation, in which all of the precipitation is attributed to convective-scale motions and mesoscale vertical motions are ignored, although it seems physically unlikely, is commonly assumed.

In Case I, the precipitation efficiency of the convective-scale motions (region C of Fig. 2), given by the ratio of the rainfall (R) to the amount of water condensed in convective updrafts (1.35 R), is 74%. Half of the remaining 26% of the total condensate (0.18 R) is re-evaporated in convective-scale downdrafts while the other half is lost to the large-scale environment (Fig. 2). This water budget for the convective-scale motions is the same as the one used by Houze and Leary (1976).

b. Case II

Case II (Fig. 3) assumes that all the water that falls in region M was condensed in a mesoscale updraft. This case requires the maximum possible amount of mesoscale lifting, since none of the precipitation in the mesoscale horizontally uniform rain area M is attributed to the transport of condensate from region C to M. Cases I and II, then, are opposite extremes in that Case I has no mesoscale lifting and Case II has the maximum possible.

In Case II, the precipitation efficiency of the convective-scale motions is again assumed to be 74%. The total condensate produced in convective updrafts is reduced to 0.81R in Case II from 1.35R in Case I (Fig. 2) because in Case II only the 0.6R falling from region C is produced in convective updrafts.

In addition to its mesoscale updraft, Case II (Fig. 3) contains a mesoscale downdraft in the lower troposphere of region M, as is always

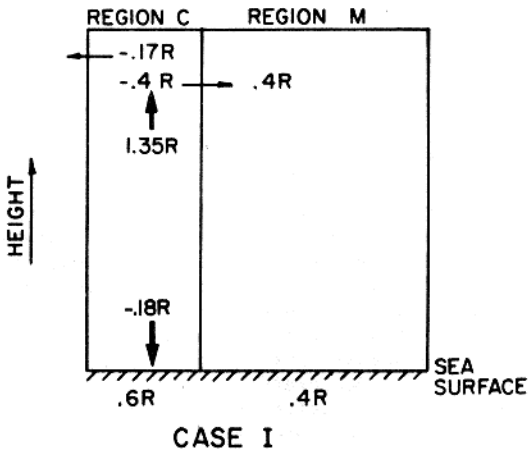

Figure 2. Schematic vertical cross-section of the hypothetical mesoscale system showing sources (positive) and sinks (negative) of condensed water for the case that assumes the absence of mesoscale vertical air motions. R represents 4.5 x 10^{12} kg. Heavy black arrows represent condensation and evaporation in convective-scale updrafts and downdrafts, respectively. Where necessary, the values used in the computations described in the text have been rounded down in the figure to obtain a water balance accurate to two significant figures.

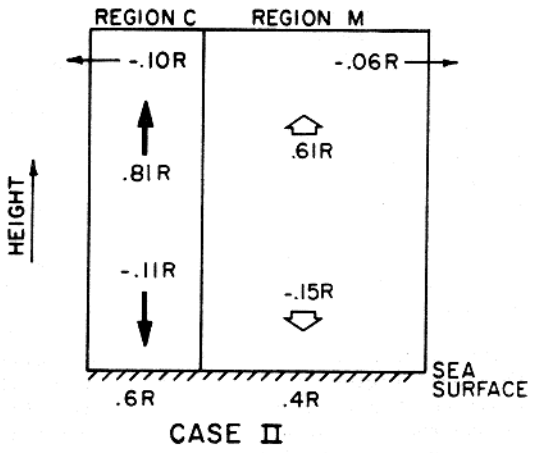

Figure 3. Same as Fig. 2 for the case that assumes all of the rain that falls in the mesoscale region is condensed in a mesoscale updraft. Outlined arrows represent condensation and evaporation in a mesoscale updraft and downdraft, respectively.

observed in such mesoscale regions as the one represented by M. The mesoscale updraft in region M, therefore, must condense enough water (specifically, 0.615R) to allow a portion to be re-evaporated in a lower tropospheric mesoscale downdraft and another portion to be lost to the large-scale environment. In Cases II, III and IV, we assume that the mesoscale downdraft evaporates 0.154R, which is equal to 39% of the amount of water, 0.4R, that finally reaches the surface as precipitation in region M. We also assume in Cases II, III and IV that the amount equal to 15% of 0.4R (or 0.06R) is lost to the large-scale environment from region M.

In Case II, the convective-scale downdrafts in region C are assumed to re-evaporate 13% of the total water condensed in convective-scale updrafts. This ratio of re-evaporation in convective-scale downdrafts to condensation in convective-scale updrafts is the same as was assumed in Case I, and, for simplicity, the same ratio will also be used in Cases III and IV.

c. Case III

Case III (Fig. 4) includes a mesoscale downdraft in the horizontally uniform mesoscale rain area (in recognition of observational evidence), but assumes that no mesoscale updraft occurs. Consequently, as in Case I, some condensate produced in region C must be transported from region C to region M to account for the 0.4R of precipitation falling from region M. The amount of water transported horizontally from region C to M (0.615R in Fig. 4), however, has to exceed 0.4R to allow for some of the transported condensate (0.154R) to evaporate in the lower-tropospheric mesoscale downdraft as it falls toward the surface, and for some condensate (0.06R) to be lost to the environment from region M. This is a greater horizontal transport from C to M than was required in Case I (Fig. 2), where there was no re-evaporation in the mesoscale downdraft.

In Case III, the precipitation efficiency of the convective-scale motions, given by the ratio of R to the total condensation (1.52R) in convective updrafts, is 66%, as compared with 74% in Case I. This drop in efficiency arises because the convective updrafts in region C of Case III have to produce additional condensate to compensate for re-evaporation in the mesoscale downdraft.

d. Case IV

In Case IV (Fig. 5) the precipitation in the mesoscale region M is accounted for partially by a mesoscale updraft within the upper troposphere of region M itself and partly by horizontal transport of 20% of the convectively-produced condensate from region C to M. Consequently, the mesoscale lifting in M is more moderate than in Case II, and the horizontal transport from region C to region M is more moderate than in Cases I or III. Case IV is, therefore, perhaps more realistic than any of the three foregoing cases. The precipitation efficiency of the convective-scale motions in Case IV, 60%, is the lowest of any of the four cases, and most nearly approaches the rather low precipitation efficiencies reported by Braham (1952) for isolated precipitating cumulonimbus clouds.

3. ESTIMATES OF MESOSCALE VERTICAL AIR MOTIONS

In order to calculate the mass and heat transports accomplished by mesoscale vertical air motions, it is first necessary to specify profiles of the mesoscale vertical velocities. These velocities are too small to be measured directly, so they must be inferred.

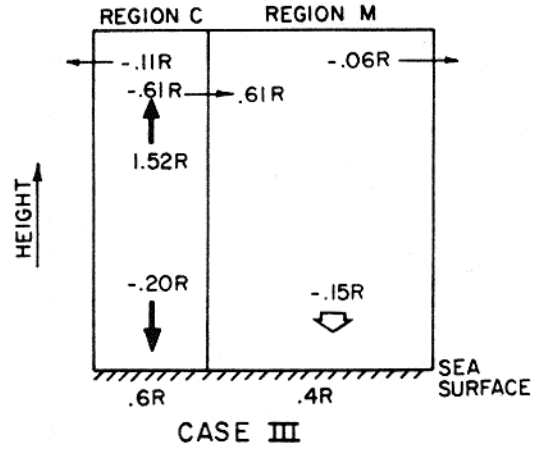

Figure 4. Same as Figs. 2 and 3 for the case that assumes the absence of a mesoscale updraft but the presence of evaporation in a mesoscale downdraft.

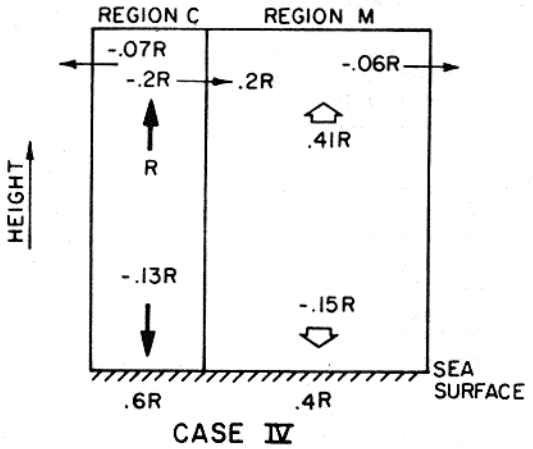

Figure 5. Same as Figs. 2 and 3 for the case that assumes the presence of condensation and evaporation in a mesoscale updraft and downdraft, respectively, as well as transport of water condensed in region C to region M.

The vertical velocity profile shown by the solid line in Fig. 6 was obtained from Brown's (1974) modelling results, and represents the average mesoscale vertical air motions in the mesoscale region. Since his model assumes that no cumulus clouds grow higher than 426 mb (7.1 km), the profile for the mesoscale updraft cannot be applied directly to our four cases, which are designed to correspond to cases in which cumulus updrafts reach heights of 14 km. The shapes and magnitudes of the profiles, however, do provide insight for constructing plausible profiles for our cases. One particularly interesting feature of Brown's profile is the close coincidence of the

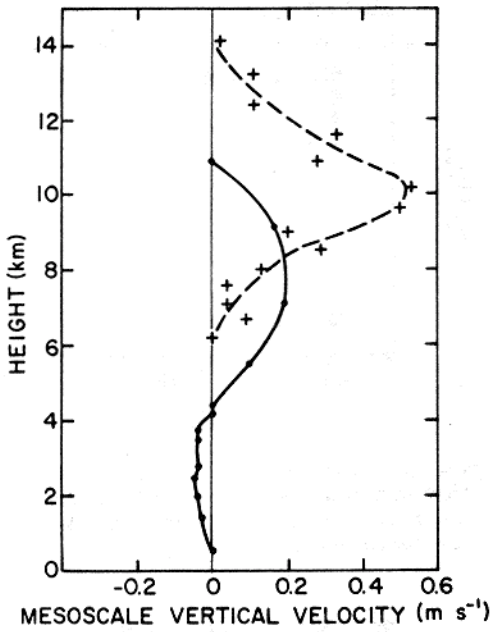

Figure 6. Mesoscale vertical velocity profiles obtained from Brown's (1974) model results (black dots and solid line), and from rawinsonde data (crosses and dashed line).

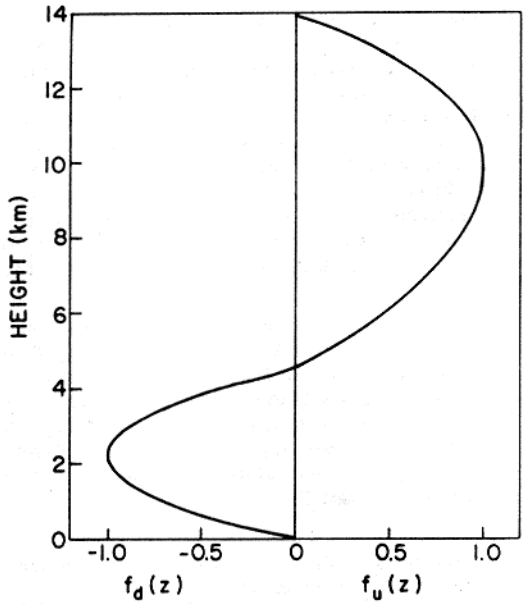

Figure 7. Normalized mesoscale vertical velocity profiles chosen for calculating the eddy fluxes of mass and heat due to mesoscale vertical air motions.

base of the mesoscale updraft and the top of the mesoscale downdraft with the melting level which was at about 4.5 km. This result, together with the cooling rates observed by Leary and Houze (1978a) at the melting level due to the melting of falling hydrometeors, leads us to select 4.5 km as the base of our model's mesoscale updraft and the top of our model's mesoscale downdraft.

Another estimate of the profile of vertical velocity in a mesoscale updraft was obtained from the time series of vertical profiles of equivalent potential temperature (Θ_e) obtained from rawinsonde soundings in the mesoscale region of the squall-line system described by Houze (1977). Using the equation for the rate of change of Θ_e in a coordinate system which is stationary with respect to the moving squall-line system, we obtain the relationship

$$w = \frac{\frac{u_R}{u_s}\frac{\partial \theta_e}{\partial t}}{\frac{\partial \theta_e}{\partial z}} \qquad (1)$$

where w is the vertical velocity in the mesoscale updraft, u_R is the relative velocity normal to the squall-line, and u_s is the velocity of propagation of the squall-line system. We have neglected advection of Θ_e parallel to the squall-line, and we have assumed that the Θ_e-field moving with the system is steady-state over the time interval between soundings. The profile shown by the crosses and the dashed line in Fig. 6 was obtained from two soundings separated by an interval of three hours. The ratio of relative wind velocity to squall-line propagation speed was obtained using the wind analyses of Houze (1977) and the winds at the times of the two soundings. The convective updrafts in that system, on average, reached heights of at least 14 km, in keeping with the greater height of the velocity maximum, as compared to the profile derived from Brown's model results.

Based on the shapes of the curves shown in Fig. 6, we have chosen parabolic profiles for the velocities of the mesoscale updraft and downdraft. These profiles, with their maximum magnitudes normalized to ± 1, are illustrated in Fig. 7. Using these profiles, it is then possible to obtain, using the water budgets of §2 and the equation for the time rate of change of water vapor mixing ratio, the magnitudes of the mesoscale vertical motions for each of the two cases that contain a mesoscale updraft.

Ignoring horizontal advection of water vapor, and integrating the equation for the time rate of change of water vapor from the base to the top of the mesoscale updraft, we obtain the relationship

$$w'_{mu} = \frac{-C + S}{\int_{4.5\,km}^{14\,km} \rho f_u(z) \frac{\partial q}{\partial z}\, dz} \qquad (2)$$

where w'_{mu} is the maximum vertical velocity in the mesoscale updraft, C is the total condensate in a unit column of air, S is the amount of water vapor lost to the large-scale environment from this column, ρ is air density, $f_u(z)$ is the shape profile of the mesoscale updraft illustrated in Fig. 7, and q is the water vapor mixing ratio. The mesoscale updraft is assumed to be saturated, since the anvil cloud is located there. The temperature in the mesoscale updraft region is assumed to be 1K warmer than the large-scale environment. This value was chosen on the basis of Brown's (1974) modelling results. We also assume that the quantity of water vapor lost to the environment in the mesoscale region is equal to the amount of condensate in the mesoscale region which is lost to the environment. The

values of w'_{mu} for the mesoscale updraft derived in this way are 69 cm s^{-1} for Case II, the situation with the maximum mesoscale uplift, and 46 cm s^{-1} for the more realistic Case IV. This value is quite close to the 53 cm s^{-1} maximum vertical velocity derived from vertical soundings in the 4-5 September 1974 squall-line system (Fig. 6).

We perform an analogous computation to determine w'_{md}, the absolute value of the maximum vertical velocity in the mesoscale downdrafts of Cases II, III, and IV. For the downdraft, we use the equation

$$w'_{md} = \frac{E}{\int_0^{4500\,m} \rho f_d(z) \frac{\partial q}{\partial z} dz} \qquad (3)$$

where E is the total evaporation in a unit column of air, and $f_d(z)$ is the downdraft velocity profile shown in Fig. 2. E is the same for Cases II, III, and IV. We chose values of $\partial q/\partial z$ to be consistent with the observations of Zipser (1977) and Houze (1977). We assume a mixing ratio equal to that at saturation at a temperature 2K colder than the environmental temperature at the top of the downdraft, increasing downward linearly to 60% of saturation at the environmental temperature at 2250 m, and increasing to 75% of saturation at the environmental temperature at 600 m. These assumptions produce the characteristic onion or diamond-shaped sounding noted by Zipser (1977) in the region of the mesoscale downdraft. Below 600 m, $\partial q/\partial z$ was chosen to be 2.5 x $10^{-6} m^{-1}$, in agreement with the boundary layer observations described by Houze (1977). For simplicity, we neglected evaporation from the sea surface and the loss of water vapor to the larger scale environment.

The maximum vertical velocity in the mesoscale downdraft, using the above equation, is calculated to be 6.3 cm s^{-1}. This agrees well (see Fig. 6) with the model results of Brown (1974).

4. CALCULATIONS OF VERTICAL EDDY FLUXES OF MASS AND MOIST STATIC ENERGY IN THE HYPOTHETICAL MESOSCALE SYSTEM DUE TO CONVECTIVE-SCALE MOTIONS

The total vertical eddy flux of mass in the hypothetical mesoscale system can be defined as:

$$M = M_{cu} + M_{cd} + M_{mu} + M_{md} \qquad (4)$$

where M_{cu} is the mass flux due to convective-scale updrafts, M_{cd} is the mass flux due to convective-scale downdrafts, M_{mu} is the mass flux due to the mesoscale updraft, and M_{md} is the mass flux due to the mesoscale downdraft.

The convective-scale contributions to the total eddy flux of mass, M_{cu} and M_{cd}, were calculated using the one-dimensional cumulus model of Austin and Houze (1973) and Houze and Leary (1976) with modifications described by Cheng and Houze (1978). We assume that all the convective updrafts in region C reach a height of 14 km, and that cloud base is located at 500 m. The large-scale area for which the vertical eddy fluxes of mass and heat are computed is chosen to be 2 x $10^5 km^2$. The environment of the mesoscale system is assumed to have the same vertical temperature and humidity profile as that observed during Phase III of the Global Atmospheric Research Programme's Atlantic Tropical Experiment (GATE).

Fig. 8 shows the results of these calculations. The vertical eddy flux of mass in convective-scale updrafts and downdrafts is directly proportional to the total amount of water condensed in region C. Since Case III (Fig. 8c), with a mesoscale downdraft but no mesoscale updraft, produces the most condensate in region C, it has the greatest convective-scale mass transports. Likewise, Cases I (Fig. 8a), IV (Fig. 8d), and II (Fig. 8b), with successively smaller amounts of condensation in region C, have successively smaller vertical eddy fluxes of mass due to convective-scale updrafts and downdrafts.

The total vertical eddy flux of moist static energy in the hypothetical mesoscale system can be defined as:

$$F = F_{cu} + F_{cd} + F_{mu} + F_{md} \qquad (5)$$

where F_{cu}, F_{cd}, F_{mu}, and F_{md} are the vertical eddy fluxes of moist static energy due to convective-scale updrafts, convective-scale downdrafts, the mesoscale updraft, and the mesoscale downdraft, respectively. These are defined by the equations:

$$F_{cu} = M_{cu}(h_{cu} - h_e) \qquad (6)$$

$$F_{cd} = M_{cd}(h_{cd} - h_e) \qquad (7)$$

$$F_{mu} = M_{mu}(h_{mu} - h_e) \qquad (8)$$

$$F_{md} = M_{md}(h_{md} - h_e) \qquad (9)$$

where h_{cu}, h_{cd}, h_{mu}, h_{md}, and h_e are values of the moist static energy in the convective-scale updrafts, convective-scale downdrafts, mesoscale updraft, mesoscale downdraft, and environment, respectively, and h, the moist static energy, is given by:

$$h = C_p T + gz + Lq \qquad (10)$$

where C_p is the specific heat of dry air, T the temperature, L the latent heat of vaporization of water, q water vapor mixing ratio, and g gravitational acceleration. Values of h_{cu} and h_{cd} are also obtained using the method of Austin and Houze (1973), Houze and Leary (1976), and Cheng and Houze (1978).

The results of these computations are shown in Fig. 9. For all four cases, the convective-scale downdrafts contribute negatively through most of their depth to the vertical eddy flux of moist static energy, because, being saturated, they are considerably moister, although somewhat cooler, than the environment. Since the magnitudes of the convective-scale fluxes of moist static energy are directly proportional to the eddy fluxes of mass, Case III again shows the greatest convective-scale flux (Fig. 9c) and Case II (Fig. 9b) the least.

5. CALCULATIONS OF VERTICAL EDDY FLUXES OF MASS AND MOIST STATIC ENERGY IN THE HYPOTHETICAL MESOSCALE SYSTEM DUE TO MESOSCALE MOTIONS

The mesoscale contributions to the vertical

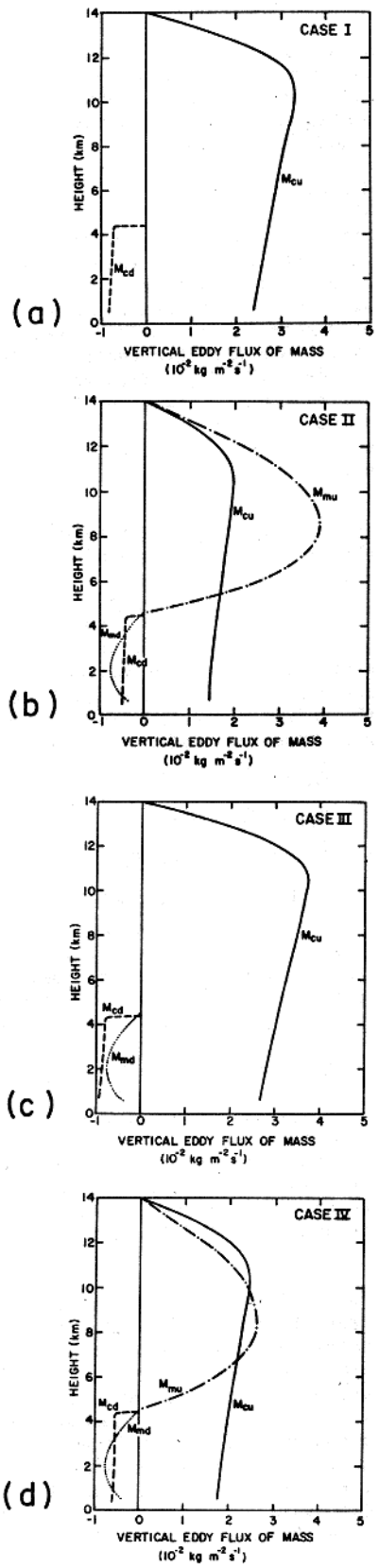

Figure 8. Vertical eddy flux of mass due to convective-scale updrafts (M_{cu}), convective-scale downdrafts (M_{cd}), mesoscale updraft (M_{mu}), and mesoscale downdraft (M_{md}). (a) Case I, (b) Case II, (c) Case III, (d) Case IV.

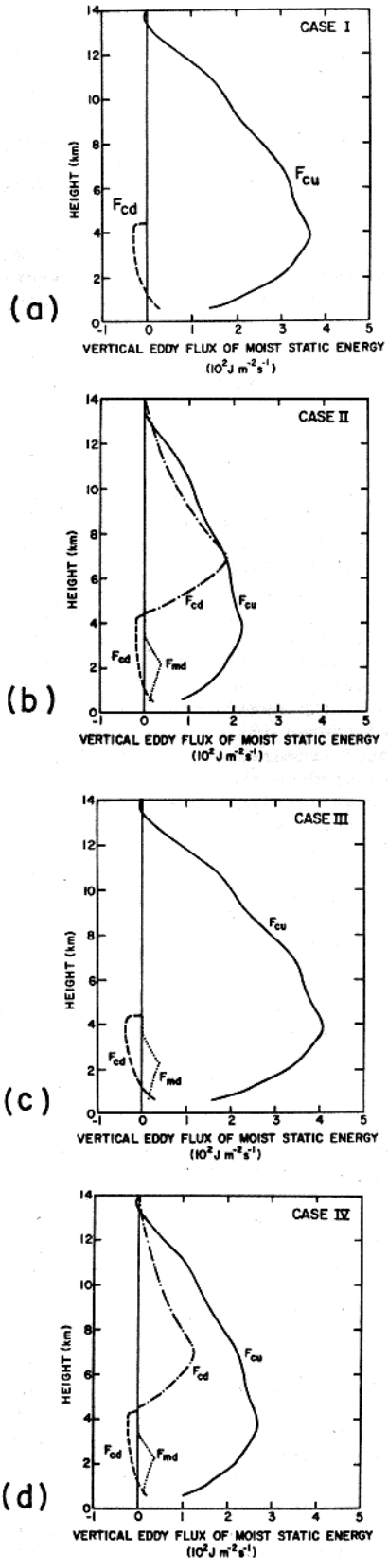

Figure 9. Vertical eddy flux of moist static energy due to convective-scale updrafts (F_{cu}), convective-scale downdrafts (F_{cd}), mesoscale updraft (F_{mu}), and mesoscale downdraft (F_{md}). (a) Case I, (b) Case II, (c) Case III, (d) Case IV.

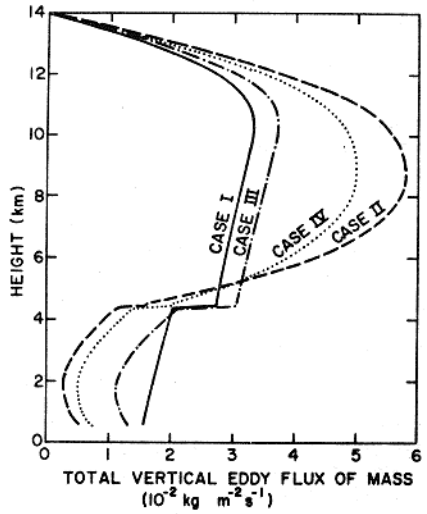

Figure 10. Total vertical eddy flux of mass due to convective-scale and mesoscale vertical air motions in the mesoscale precipitation system for Cases I, II, III and IV.

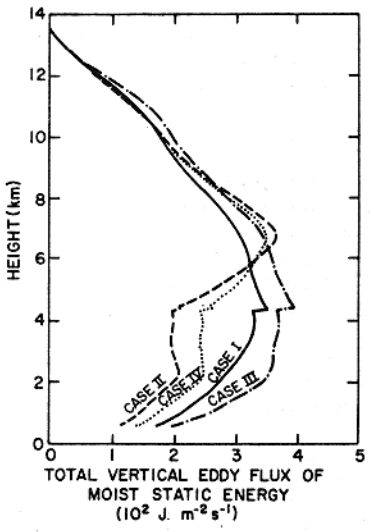

Figure 11. Total vertical eddy flux of moist static energy due to both convective-scale and mesoscale vertical air motions in the mesoscale precipitation system for Cases I, II, III and IV.

eddy flux of mass were calculated using the equations:

$$M_{mu} = \rho w'_{mu} f_u(z) \frac{A_m}{A \Delta t} \quad (11)$$

and

$$M_{md} = \rho w'_{md} f_d(z) \frac{A_m}{A \Delta t} \quad (12)$$

where A_m is the area occupied by region M, A is the large-scale area over which the fluxes are computed ($2 \times 10^5 km^2$), and Δt is the lifetime of the mesoscale updraft and downdraft. The results of these calculations are shown in Fig. 8. Since w'_{md} is the same (6.3 cm s^{-1}) for the three cases (II, III, and IV) possessing mesoscale downdrafts, the eddy fluxes of mass are the same.

The mesoscale downdraft makes a negative contribution to the total eddy flux of mass similar in magnitude to that of the convective-scale downdrafts. The mesoscale updraft makes a positive contribution to the vertical eddy flux of mass of similar magnitude in the upper troposphere to that of the convective-scale updrafts. Case II, with the larger w'_{mu}(69 cm s^{-1}) has a proportionally larger M_{mu} than Case IV, for which w'_{mu} is 46 cm s^{-1}.

The mesoscale contributions to the vertical eddy fluxes of moist static energy were calculated using (8) and (9). The moist static energy of the mesoscale updraft and downdraft were calculated using the assumptions described in §3. The temperature in the mesoscale downdraft was assumed to be 2K colder than the environment at 4500 m, the top of the downdraft. This temperature deviation decreased linearly with decreasing height to zero at 3600 m. Both Zipser (1977) and Houze (1977) observed this layer of cool air at the top of the mesoscale downdraft. We attribute it to the cooling due to melting hydrometeors as described by Leary and Houze (1978a). Below 3600 m we assumed that the temperature in the mesoscale downdraft was the same as that in the environment.

The results of the computations of the mesoscale vertical eddy fluxes of moist static energy are shown in Fig. 9. The mesoscale downdraft, drier and at some levels colder than the environment, contributes positively to the vertical eddy flux of moist static energy, and partially offsets the negative vertical eddy flux in the convective-scale downdrafts. The mesoscale updraft makes a significant contribution to the total vertical eddy flux of moist static energy in Cases II (Fig. 9b) and IV (Fig. 9d).

6. TOTAL VERTICAL EDDY FLUXES OF MASS AND MOIST STATIC ENERGY

Figs. 10 and 11 show the total vertical eddy fluxes of mass and heat, respectively, for the hypothetical mesoscale precipitation system in each of the four cases, including both convective-scale and mesoscale vertical air motions. In the upper troposphere, Cases II and IV, which possess both mesoscale and convective-scale updrafts, have the largest vertical eddy fluxes of mass (Fig. 10). In the lower troposphere, however, Cases II and IV have the smallest vertical eddy fluxes of mass, because both these cases also possess a mesoscale downdraft.

The total vertical fluxes of moist static energy (Fig. 10) show a different pattern. Above 8 km there is very little difference among the four cases. The greater mass fluxes in Cases II and IV above 8 km due to the presence of mesoscale updrafts are largely offset by the greater efficiency of the warmer convective-scale updrafts in transporting moist static energy.

In the lower troposphere below 6 km, the four cases show less similarity. Case I, the case commonly assumed in calculating vertical eddy fluxes, and Case IV, the case chosen to be most realistic, lie between the extremes provided by the curves describing Cases II and III. This suggests that the high precipitation efficiency calculated

by Johnson (1976) and assumed by Houze and Leary (1976) when mesoscale vertical air motions are ignored, is in effect a parameterization of the vertical eddy fluxes they accomplish.

7. CONCLUSIONS

We have obtained estimates of the magnitudes of mesoscale vertical air motions in intense tropical convection, based on the case studies of Houze (1977) and Zipser (1977), the modelling results of Brown (1974), and assumed water budgets for a hypothetical mesoscale precipitation system. Our estimates of the maximum vertical velocity in the mesoscale updraft fall between 20 and 70 cm s^{-1}. In the weaker mesoscale downdraft our calculations show a maximum vertical velocity less than 7 cm s^{-1}.

The melting level is closely related to the top of the mesoscale downdraft. We suggest that cooling there, due to the melting of frozen hydrometeors, triggers the mesoscale downdraft, which is maintained as the air sinks by the cooling due to the evaporation of falling rain.

Mesoscale updrafts and downdrafts make important contributions to the vertical eddy fluxes of mass and moist static energy, comparable in magnitude to those accomplished by convective-scale motions. The high precipitation efficiencies calculated (or assumed) when mesoscale vertical air motions are ignored compensate to some extent for neglecting mesoscale air motions in computations of the vertical eddy fluxes of mass and moist static energy.

ACKNOWLEDGMENTS

We thank C.-P. Cheng for his assistance with the computer program which calculated the convective transports of mass and heat. We also thank Thomas J. Matejka and Peter V. Hobbs for reading the manuscript. This research was supported by the Global Atmospheric Research Program, National Science Foundation, and the U.S. GATE Project Office, National Oceanic and Atmospheric Administration, Grant ATM74-14830.

REFERENCES

Abercromby, R., 1887: *Weather.* D. Appleton and Company, 472pp. (see p. 248)

Austin, P.M., and R.A. Houze, Jr., 1973: A technique for computing vertical transports by precipitating cumuli. *J. Atmos. Sci.*, *30*, 1100-1111.

Brown, J.M., 1974: Mesoscale motions induced by cumulus convection: a numerical study. Ph.D. thesis, Massachusetts Institute of Technology, 206 pp.

Braham, R.R. Jr., 1952: The water and energy budgets of the thunderstorm and their relationship to thunderstorm development. *J. Meteor.*, *9*, 227-242.

Cheng, C.-P., and R.A. Houze, Jr., 1978: Average convective fluxes in the Intertropical Convergence Zone. Manuscript in preparation.

Hamilton, R.A., and J.W. Archbold, 1945: Meteorology of Nigeria and adjacent territory. *Quart. J. Roy. Meteor. Soc.*, *71*, 231-262.

Houze, R.A., Jr., 1977: Structure and dynamics of a tropical squall-line system. *Mon. Wea. Rev.*, *105*, 1540-1567.

_____, and C.A. Leary, 1976: Comparison of convective mass and heat transports in tropical easterly waves computed by two methods. *J. Atmos. Sci.*, *33*, 424-429.

Humphreys, W.R., 1914: The thunderstorm and its phenomena. *Mon. Wea. Rev.*, *42*, 348-380.

Johnson, R.H., 1976: The role of convective-scale precipitation downdrafts in cumulus and synoptic-scale interactions. *J. Atmos. Sci.*, *33*, 1890-1910.

Leary, C.A., and R.A. Houze, Jr., 1978a: Observations of horizontally uniform precipitation and radar bright bands in the tropics. *Preprints 18th Conference on Radar Meteorology*, Amer. Meteor. Soc., Boston, 1978, 1-8.

_____, and _____, 1987b: Response of the large-scale wind field to a cloud cluster in the ITCZ. Manuscript in preparation.

_____, and _____, 1978c: The structure and evolution of deep convection in a tropical cloud cluster. Manuscript in preparation.

Yanai, M., S. Esbensen, and J.-H. Chu, 1973: Determination of the bulk properties of tropical cloud clusters from large-scale heat and moisture budgets. *J. Atmos. Sci.*, *30*, 611-627.

Zipser, E.J., 1969: The role of organized unsaturated convective downdrafts in the structure and rapid decay of an equatorial disturbance. *J. Appl. Meteor.*, *8*, 799-814.

_____, 1977: Mesoscale and convective-scale downdrafts as distinct components of squall-line circulation. *Mon. Wea. Rev.*, *105*, 1568-1589.